

# Reduced loss and bend sensitivity in hermetically-sealed hollow-core fiber gas cells using gas-induced differential refractive index

Somarpita Pradhan,\* Thomas W. Kelly, D Elizaveta ELISTRATOVA, IAN A. DAVIDSON, D PETER HORAK, D AND NATALIE V. WHEELER

Optoelectronics Research Centre, University of Southampton, Southampton SO17 1BJ, United Kingdom \*S.Pradhan@soton.ac.uk

**Abstract:** Hollow-core optical fiber (HCF) gas cells are an attractive option for many applications including metrology and non-linear optics due to the enhanced gas-light interaction length in a compact and lightweight format. Here, we report the first demonstration and characterization of a selectively pressurized, hermetically sealed hollow-core fiber-based gas cell, where the core is filled with a higher gas pressure than the cladding to enhance the optical performance. This differential gas pressure creates a gas-induced differential refractive index (GDRI) that is shown to enable significant modification of the HCF's optical performance. Measurements on fabricated gas cells indicate a significant broadband reduction in attenuation of up to ~10 dB (at 1100 nm) for a 24 m fiber length and an estimated pressure difference of ~6 bar between the gas in the core and cladding regions. Additionally, using the fabricated gas cells, we show experimentally for the first time that GDRI can reduce macrobend loss in HCFs. Finally, long term (one year) measurements indicate no degradation in the gas cell performance due to gas permeation or gas exchange between the core and cladding regions, demonstrating the viability of using this gas cell format to implement a GDRI within a HCF to improve optical performance over an extended time period in an all-fiber format.

Published by Optica Publishing Group under the terms of the Creative Commons Attribution 4.0 License. Further distribution of this work must maintain attribution to the author(s) and the published article's title, journal citation, and DOI.

#### 1. Introduction

Since the first demonstrations of a hollow-core optical fiber (HCF) [1] and the possibility of low-loss light transmission through hollow-core structures [2], extensive attention has been focused on utilizing them for diverse applications. While there is high interest in the potential of HCFs for data transmission [3,4] due to their ultimate low latency, non-linearity, and loss [5,6], the enhanced gas-light interaction length provided by the simultaneous confinement of light and gas within the hollow core makes them ideal for a range of other applications including high sensitivity gas detection [7–9], nonlinear optics [10,11] and frequency metrology [12]. The core of a HCF can be filled with a gas sample to create a compact gas cell and several different methods for integrating HCFs into hermetically sealed all-fiber gas cells have been demonstrated [12,13]. Key challenges in the fabrication of HCF gas cells are controlling the gas pressure within the hollow regions of the fiber and sealing the two ends in a hermetic manner, while maintaining low insertion loss. By splicing both ends of a gas-filled HCF to all-solid fiber, a hermetically-sealed gas cell can be fabricated with low insertion loss and no need for bulk optic alignment; moreover, this gas cell can be easily interconnected with other optical fiber components [14,15]. Up until now, the HCF-based gas cells that have been reported have been fabricated by filling both the core and cladding regions of the HCF simultaneously, with the same gas composition at the same pressure. However, independent control of the gas pressure and/ or composition within the

#545939 Received 30 Oct 2024; revised 14 Dec 2024; accepted 18 Dec 2024; published 7 Jan 2025

core and cladding of the fiber adds an extra degree of freedom to tune the optical properties of HCF-based gas cells.

Recently, it has been reported that by creating a gas-induced differential refractive index (GDRI) between the core and cladding of a HCF, the fiber's optical properties such as attenuation, bend loss and modality can be significantly modified [16]. Practically, it was demonstrated that a very small refractive index change introduced by selectively filling the core with higher gas pressure than the cladding can lead to significant improvement in the fiber attenuation. This method introduced a new approach to tailor HCF characteristics post-fabrication, with the potential to attain performance metrics that are otherwise challenging (or potentially impossible) to achieve due to fiber design and fabrication constraints [17,18]. However, in [16], the differential pressure required to create the GDRI was delivered by collapsing the cladding region at the distal end of the HCF and subsequently using a bulk gas chamber to selectively pressurize the core region; this arrangement resulted in high insertion loss, a bulky arrangement, and a non-uniform pressure profile along the HCF.

Here, we demonstrate a novel technique to employ GDRI in a hermetically sealed, all-fiber HCF-based gas cell via an approach which enables selective-core filling to achieve the differential gas pressure required and implement a splicing routine whereby there is no gas exchange between the core and the cladding regions of the fiber, so the differential pressure is maintained. We confirm this by comparing optical measurements before and after gas-filling and demonstrate an increase in transmission of up to  $\sim 10$  dB at 1100 nm [19]. Furthermore, we report the first experimental bend loss measurements of hermetically sealed and selectively pressurized gas cells and demonstrate that, as predicted in [16], the GDRI reduces bend sensitivity, thus highlighting the potential of using this gas cell format to reduce bend loss in HCFs. Long-term (12 months) optical measurements of the fabricated gas cells confirmed that this change in HCF properties is maintained, with no sign of gas permeation through the thin ( $\sim 428 \pm 30$  nm) membranes which separate the core and cladding regions of the fiber or leakage at the splices.

In Section 2, the design and fabrication of the HCF based gas cells studied in this work is described. Characteristics of the gas cells are analyzed in Section 3, specifically their optical transmission and bend loss behavior. Section 4 provides a theoretical background to discuss the origin of the observed improved optical performance of the gas cells. Finally, this work is concluded in Section 5.

## 2. Fabrication of selectively filled HCF gas cells

The air-filled regions in HCFs, the carefully arranged air holes defined by thin glass membranes, lead to their beneficial gas-light interaction properties but also make splicing them more challenging than conventional all-glass optical fibers [20,21]. In the work presented here, extra complexity is unfortunately added as, in addition to providing low optical loss and a hermetic seal between the voids in the HCF and the surrounding environment, prevention of gas exchange between the core and the cladding regions of the HCF is also required.

#### 2.1. Hollow-core fiber design

The HCF used in our experiment is a 7-element single-cladding ring ("tubular" fiber, termed 7T-HCF in this paper) hollow-core antiresonant fiber with a core diameter of  $\sim$ 20.5 µm, an outer diameter of  $\sim$ 223 µm, an average cladding hole diameter of  $\sim$ 9.43 µm and cladding membrane thickness of 428 ± 30 µm, as measured from the SEM shown in Fig. 1(a). The fiber was drawn using the standard stack-and-draw method, details of which can be found in [22]. The fiber design was optimized for applications in the visible region with a minimum attenuation of 23.6 dB/km at 570 nm [22], and thus its loss in the near-infrared (near-IR) region is much higher in comparison (0.6 dB/m at 1310 nm) as measured using the cutback technique [19]. While this near-IR loss is significantly higher than state-of-the-art HCFs [e.g., 23], this fiber provides an

ideal testbed for exploring the potential of improving the transmission properties of HCFs using GDRI due to its simple structure, as the principles shown within this work can also be applied to other, lower loss HCFs to improve their optical performance.

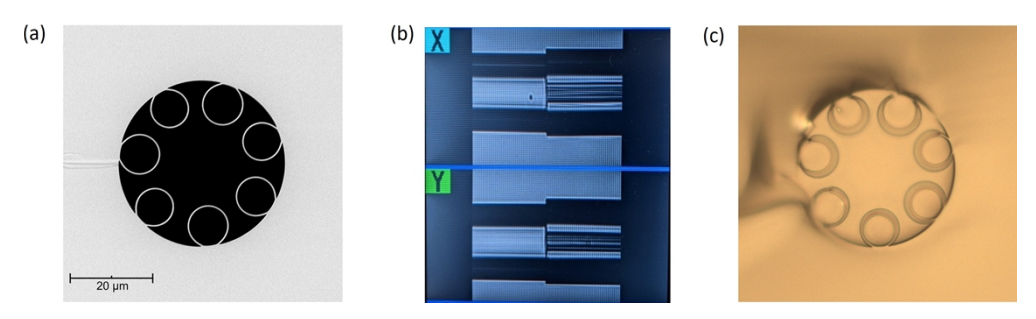


**Fig. 1.** (a) SEM image of 7T-HCF structure; (b) side-image showing spliced joint at buffer fiber-7T-HCF interface captured on Fujikura, ARCMaster-FSM-100P screen; (c) microscope image of cladding tube imprints of HCF on solid buffer fiber side to confirm good attachment after splice without deformation of the cladding tube structures.

## 2.2. Hollow-core fiber gas cell fabrication

To make a low-loss HCF gas cell, we built upon the all-fiber approach reported in [12], but with additional crucial steps to enable differential core and cladding pressure. A  $\sim$ 24 m length of the 7T-HCF was used for each gas cell; this length was selected based on the near-IR transmission of the fiber, to ensure any improvements in the loss of the fiber due to GDRI are easily detected, while also ensuring the gas filling times are reasonably short (as gas filling times scale with fiber length squared) [24]. The method reported, and validated here, can also be directly applied to longer fiber lengths albeit with longer fill times.

To enable the all-fiber format, during the cell fabrication process, the HCF is fusion-spliced (Fujikura, ARCMaster-FSM-100P) to a solid-core fiber (SCF) at both ends. There are several key considerations when selecting the SCF including the core diameter, mode field diameter (MFD), numerical aperture (NA), and outer diameter (OD) to ensure a strong and low loss splice, as well as the practicality of what SCFs are available. Furthermore, due to the presence of the thin glass membranes that define the cladding structure, the splice parameters need to be carefully selected and controlled to reduce the insertion loss of the final cell. Given that the MFD and OD of the 7T-HCF are  $\sim 14.4$  and 223  $\mu$ m respectively, we chose to splice the HCF to conventional SMF (corning SMF-28) via a  $\sim 1$  m length of a commercially obtained, custom buffer fiber with a core diameter of 20  $\mu$ m and OD of 200  $\mu$ m. The buffer fiber is not perfectly mode-matched (MFD  $\sim 18.9~\mu$ m at 1200 nm) but well matched in terms of NA (0.06), and outer diameter. Calculation suggests the minimum splice loss at 1200 nm (without any structural deformation) will be  $\sim 0.5$  dB (due to a MFD mismatch loss of 0.32 dB and Fresnel reflection of  $\sim 0.15$  dB).

An effective splicing recipe for these fibers was developed and tested by measuring the impact of varying the splicing parameters such as arc time, fusion power, overlap factor and heat offset on both the optical performance and splice strength. A balance was established which enabled acceptable optical loss (~ 1 dB per splice) without visible collapse or deformation of the microstructure and good mechanical strength (determined qualitatively by investigating the ease with which the splice could be broken while imaging the imprint of the HCF on the end face of the SCF).

As it is necessary to control the core and cladding pressure of the fiber separately in this work, which is not normally relevant or investigated for HCF to SCF splicing, gas movement between the core and cladding regions must be prevented. Practically, for the splice connection, this

requires that the cladding tubes are securely fused to the buffer fiber; whereas in a standard HCF to SCF splice this may not be the case, as the splice performance can be adequate with only the outer jacket of the HCF fused to the SCF. Here, we modified the splicing routine to ensure this strong contact between the cladding tubes and SCF, which may have resulted in the slightly increased loss ( $\sim 0.5$  dB) due to splicing, and hence the measured total splice loss of  $\sim 1$  dB. To achieve this, the overlap factor (a measure of to what extend the HCF is pushed into the solid core fiber to make the attachment firm and leakage-proof) used in the splicing recipe was set to  $10~\mu m$ . Strong attachment was confirmed by breaking a series of test splices after fusing and observing the SCF side under a microscope. For a suitable splice, the image of the cladding tube imprints from the HCF could be clearly seen on the solid fiber. Figure 1(b) shows a side image of a typical splice, alongside an image of the imprint of the cladding tubes on the buffer fiber side (Fig. 1(c)) after breaking the splice joint. These images confirm good attachment of the cladding tubes of the 7T-HCF onto the solid buffer fiber side without significant deformation of the cladding tubes due to splicing.

The fabrication of each HCF gas cell is a multi-step process and the key steps are outlined schematically in Fig. 2. Firstly, a reference cell is fabricated, see Fig. 2(I.); here the gas content inside the HCF is atmospheric air at standard temperature and pressure (s.t.p). A  $\sim$ 24 m length of 7T-HCF was fusion-spliced to a buffer fiber and SMF pigtail assembly at both ends, to ensure repeatability and ease of measurement in subsequent measurements. Splicing of buffer fiber to SMF pigtail is a standard solid to solid fiber splicing where the loss contribution comes mostly from the MFD mismatch with very low splice loss ( $\sim$ 0.05 dB). The optical transmission of this reference cell was then recorded using a white light source and optical spectrum analyzer; the details are reported in Section 3.

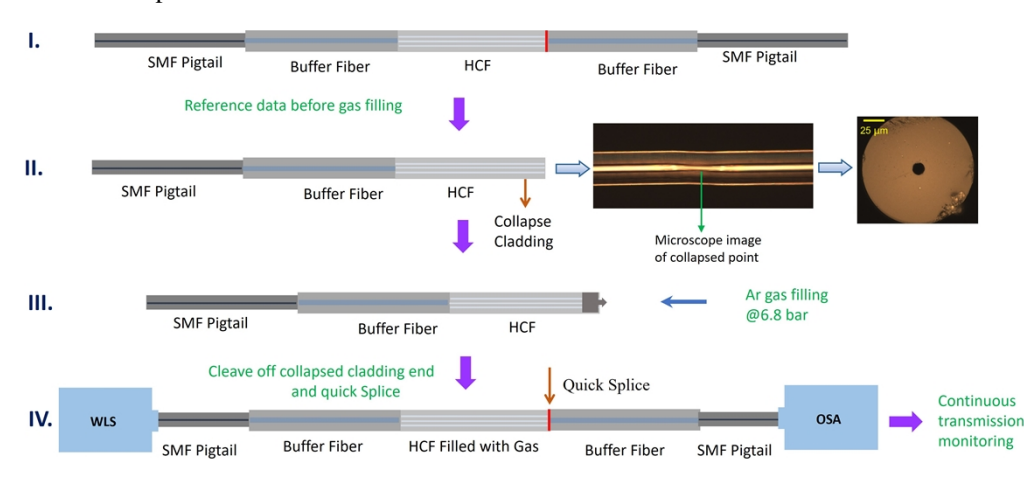


**Fig. 2.** Schematic representation of selective gas filling steps while fabricating gas cells starting from taking reference spectrum to continuous monitoring of transmission spectra of selectively filled HCF gas cells.

Following the optical measurement of the reference cell, the splice between the HCF and the buffer fiber was broken at the distal (measurement) end. The cladding tubes of the HCF at the distal end were then collapsed using a fusion splicer (Fujikura Arc fusion Splicer: FSM-50S), shown in Fig. 2(II.). This enables the core of the HCF to be selectively filled with a higher gas pressure without changing the gas composition or pressure in the cladding holes (which was atmospheric air at s.t.p. throughout the process). The core was then selectively filled with Argon at 6.8 bar gauge pressure (in  $\sim$  45 minutes) using a gas filling manifold, as depicted in Fig. 2(III.). The pressure value of 6.8 bar was chosen because, from our previous work [16], this pressure difference had been shown to be high enough to significantly modify the optical properties of the

HCF used and also because this was readily available in our laboratory. Note, after gas filling, the gas composition in the final gas cell is not 100% Argon as the fiber is not evacuated before the gas filling process. The HCF samples used in this work were left open to the atmosphere for a sufficiently long time before filling (>1 week) and therefore were initially filled with air at atmospheric pressure. However, the refractive index of Argon is very similar to air [25], so the actual impact on the resultant change in the optical properties due to the mix of Argon and air in the final cell is minimal as compared to a cell filled with pure Argon.

After gas-filling, the collapsed cladding section of the HCF was cleaved off (Fujikura, CT-101) and this end was spliced quickly to a length of buffer fiber and SMF, resulting in an all-fiber gas cell comprised of ~24 m of 7T-HCF (with a core selectively pressurized with argon gas) and hermetically spliced buffer fiber-SMF pigtails assembly at both ends, Fig. 2(IV.). Two similar gas cells have been fabricated following the same methodology for the purpose of our study. The only known difference between the fabrication of these cells is in the time taken for the quick second splice after releasing the collapsed fiber end from the gas manifold. For gas cell 1, this splice took ~90 seconds and for gas cell 2 it took ~40 seconds. The effect of this on the final core gas pressure is discussed in the following sections.

## 3. HCF gas cell characterization

All the reported optical measurements were made using a tungsten-halogen white light source (Bentham, WLS100) and optical spectrum analyzer (OSA: Yokogawa, AQ6315A) set to a 10 nm resolution, with both directly connected to the gas cells (HCF-buffer fiber-SMF pigtails assembly) via FC/APC connectors.

#### 3.1. Transmission measurements

The effect of the selective gas filling process can be seen in Fig. 3 by comparing the transmission from the reference cell (black lines in Fig. 3(a) and (b)), where the core and cladding have equal gas pressures (air at atmospheric pressure), with the transmission of the selectively-filled gas cells. Transmission data on the selectively-filled gas cells was measured immediately after fabrication (red lines), and then at different time intervals post-fabrication over the following year. These measurements are shown in Fig. 3(a) and Fig. 3(b) for gas cells 1 and 2 respectively.

The results show a substantial improvement in transmission for both gas cells when the core is selectively filled with Argon at an elevated pressure compared to the cladding. The largest increase in transmission for both gas cells immediately after fabrication is recorded at a wavelength of  $\sim 1100$  nm as 8.5 dB and 10 dB for gas cells 1 and 2 respectively. For gas cell 1, this increase in transmission then slightly reduces by  $\sim 2$  dB over the initial  $\sim$ few hours after fabrication, while for gas cell 2, the initial transmission is relatively stable, but a discrete improvement in transmission is observed after 29 days. The possible causes of these changes are discussed further in Section 4.

Following the initial changes to their transmissions, the performance of both gas cells, Fig. 3(a) and (b) show that their transmission spectra remained extremely consistent over subsequent measurements made in the following year. The dips seen in the transmission spectra of both gas cells between 1350 and 1400 nm can be attributed to water vapor absorption in the gas cell. This reduces over the ~one year time period of the measurements which is consistent with previously observed behavior in sealed HCF gas cells [26] and can be attributed to the water molecules (vapor) present in the fiber's core adsorbing to the silica walls that surround the core over time.

## 3.2. Bend loss measurements

Bend-loss measurements were performed on both selectively pressurized fiber cells  $\sim$ 12 months after their fabrication using a  $\sim$ 3 m portion of the  $\sim$ 24 m fiber length of HCF (at the OSA/distal/measurement end) to bend-diameters of 40, 32, 24, 16, 13, 8, and 4 cm respectively, with

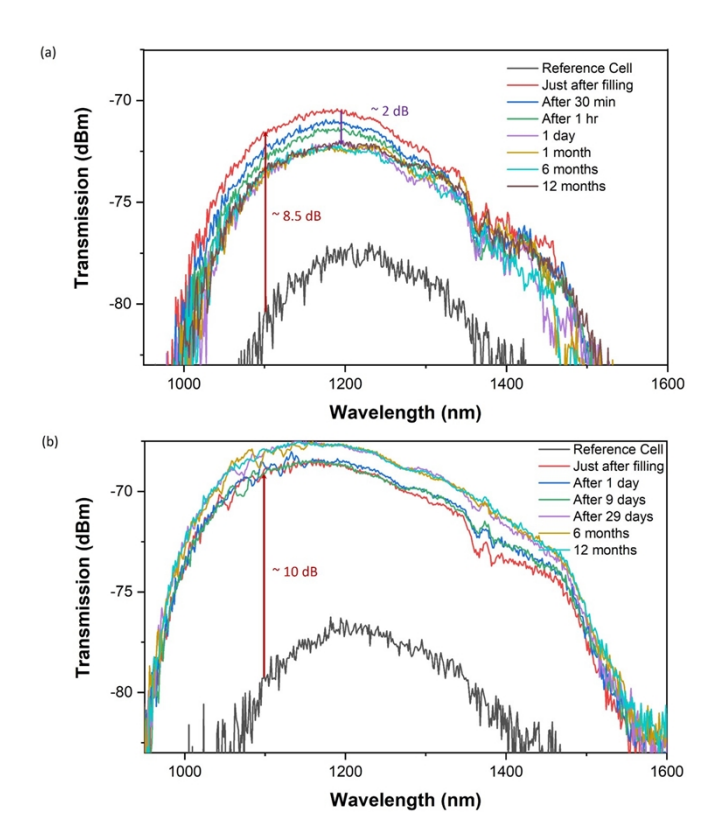


**Fig. 3.** Evolution of the recorded transmission spectra of 7T-HCF-based gas cells after filling with Argon gas over 12 months after fabrication (a) gas cell 1 (b) gas cell 2. The black lines show the reference cell transmission.

increasing number of turns as the fiber coil diameter decreases. The 3 m length was selected as it is long enough to show the significant change due to bending without risking the integrity of the gas-filled fiber cells with increasing number of turns. Taking spectra at a bend diameter  $(\phi_b)$  of 60 cm as the reference, to mimic the fiber transmission when deployed in a straight state (due to lab space constraints), the bend loss was determined for each bend diameter. After each measurement, the fiber was restored to initial condition  $(\phi_b = 60 \text{ cm})$  to ensure that any stress in the fiber is released and to recover the initial status. The same procedure was used for both gas cells, as well as a reference cell, which was not selectively pressurized. This reference cell was fabricated using the same 7T-HCF ( $\sim$ 24 m)-buffer fiber-SMF assembly, but with the core and cladding left at same pressure  $(P_{\text{atm}})$ , and bend loss measurements performed following the same procedure as the selectively-pressurized gas cells.

To investigate the additional loss encountered by the gas cells due to tight bending, a specific wavelength, 1206.8 nm, within the transmission band has been selected. This wavelength is close to the maximum transmission in the near-IR window for both cells, and its bend-sensitivity is shown in Fig. 4(a) as well as for the reference cell.

Figure 4(a) shows that the bend loss dependence of the two selectively-pressurized gas cells is slightly different at tight bend diameters, < 8 cm, but prior to this, the change in transmission is insignificant. Hence, bend-loss is negligible for gas cell 1 down to a diameter ( $\phi_b$ ) of 4 cm, resulting in a loss of only 0.32 dB/m at 1206.8 nm. Gas cell 2 shows even lower bend-sensitivity with little if any change even at 4 cm diameter (0.07 dB/m), with the change seen being close to the noise on these measurements ( $\pm 0.05$  dB/m). Furthermore, the measured bend-loss spectra

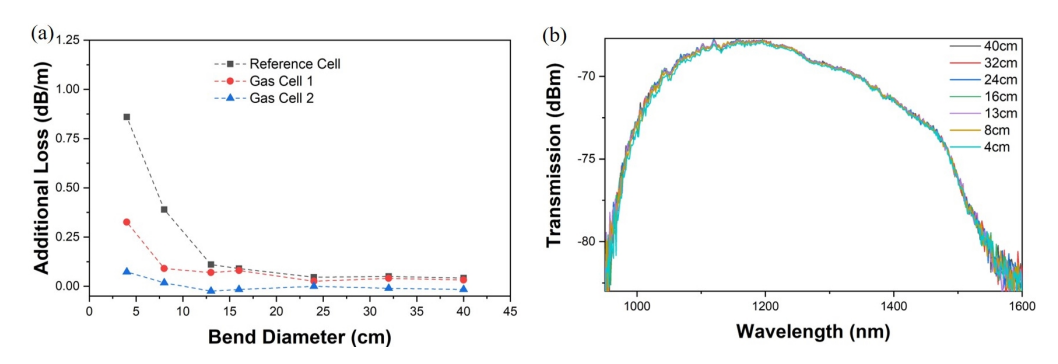


**Fig. 4.** (a) Comparison of additional loss due to bending between selectively filled 7T-HCF gas cells with unfilled reference cell at 1206.8 nm wavelength for different bend diameters of 40 cm, 32 cm, 24 cm, 16 cm, 13 cm, 8 cm and 4 cm; (b) transmission spectra of 7T-HCF gas cell 2 recorded with 3 m of fiber coiled at different bend diameters to investigate bend loss behavior.

for gas cell 2 are shown in Fig. 4(b) as an example of best bend performance of the selectively pressurized cells. Gas cell 2's bend insensitivity is clearly seen here right across its near-IR (950->1550 nm) transmission window.

Comparing this performance against the reference cell (black curve in Fig. 4(a)) the significance of the bend-loss sensitivity improvement in the selectively pressurized gas-cells (red and blue curves) can be clearly seen, as the bend-loss of the reference cell begins to increase at  $\sim$ 13 cm diameter, and reaches >0.85 dB/m at 4 cm, much higher than that seen in the selectively pressurized cells with no significant change being recorded for gas cell 2 at this bend diameter.

## 4. Discussion

The transmission spectra shown in Section 3 for the two fabricated gas cells suggest that the enhancement in optical properties is strictly dependent on the differential gas pressure between core and cladding of the HCF. Hence, perfect collapse of the cladding holes, hermetic splices, and the time taken to perform the second splice (that seals the cell) in the gas cell fabrication process play a crucial role in determining the improved characteristics.

To theoretically investigate the gas pressure profiles inside gas cells 1 and 2, after the second splice, the pressure evolution was simulated approximating the fiber core with a cylindrical tube of the fiber core diameter [27]. The simulation considered the pressure evolution during and after splicing as a 2-step process - gas leaking out before and during splicing, and pressure equalization (along the fiber's core) after the cell is sealed. Starting with a flat pressure profile of  $\sim$ 6.8 bar argon across the 24 m length of HCF, the average pressure inside the gas cell has been estimated, for the case of one open end, after a series of times, see Fig. 5(a). Based on these simulation curves, and the estimated time between removal of the cells from the pressurization system and completion of the second splice ( $\sim$ 90 seconds for cell 1,  $\sim$ 40 seconds for cell 2, as already mentioned), the final pressure profile within the fiber can be deduced.

In turn, this final profile can then be used to simulate how the pressure within the core of the HCF in the sealed gas-cells equalizes in time, and hence the final cell pressure. An example of this, for gas cell 1, is shown in Fig. 5(b), which results in a final pressure estimate of  $\sim$  5.6 bar. Following an identical process the final pressure for cell 2 is estimated to be  $\sim$  6 bar.

Using these simulated average final core gas pressures inside the fabricated gas cells, and assuming the cladding gas pressure is 1 bar atmospheric air, the effect of GDRI for this fiber configuration can be numerically simulated (using COMSOL Multiphysics) [16]. Figure 6 shows the results of these simulations and, as expected, that selective pressurization of the core reduces

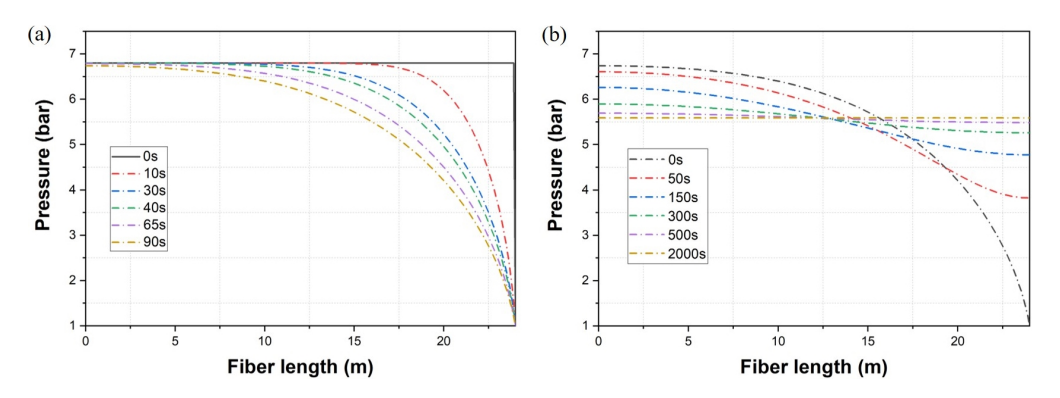


**Fig. 5.** (a) Simulated pressure profile in the fabricated, selectively-filled 7T-HCF gas cells before completion of the second (sealing) splice when filled with 6.8 bar pressure; (b) post-splice pressure equalization along the fiber length for gas cell 1.

the fiber loss (blue lines in Fig. 6(a) and (b)). The change in loss, calculated from the simulated loss values for the fiber with 1 and 5.6/6.0 bar core pressurization, are also shown in Fig. 6. Comparing this to the measured loss reduction values obtained from the fabricated gas-cells pre- and post-selective pressurization (just after filling as shown in red arrows in Fig. 3) shows good agreement to the 5.6 bar pressure estimated for cell 1 but weaker agreement with the loss obtained by simulation for cell 2 pressurized to 6.0 bar. This suggests that while the pressure estimate for cell 1 is good, the estimate for cell 2 may be less accurate. However, as the precise time between the active pressurization finishing and completion of the second splice can only be roughly estimated, due to the practicalities of the process, it is possible that the pressure in cell 2 may be higher than estimated.

An alternative explanation is that some higher order mode (HOM) content may have been excited at the input splice (between the buffer fiber and the HCF) of both cells due to mode field mismatch and/or core alignment [28]. As the simulations reported in Fig. 6 only consider the fundamental mode loss, the presence of HOM content would affect the actual loss (given these modes are much higher loss than the fundamental). From [16], GDRI will also impact (reduce in the case of a higher gas pressure in the core region than the cladding) the loss of the HOMs and therefore some HOM content could result in a higher reduction in the measured fiber's loss than predicted from the simulations that are based on the fundamental mode alone. As the excitation of HOM content is also highly dependent on the alignment of the cores in the buffer and HCFs, the amount of HOM content may vary between the cells, explaining why this is seen more in cell 2. While every care was taken to prevent core misalignment, as the precision of the splicer used is not absolute, it is hence not possible to ensure perfect alignment.

Additionally, simulated confinement loss for different core pressures is shown in Fig. 6(c) where the cladding pressure was kept fixed at 1 bar. This plot depicts that the loss in the HCF reduces with increasing differential pressure.

The transmission data reported in Fig. 3(a) for gas cell 1 shows an initial reduction in the transmission in the first few hours, consistent with a reduction in pressure difference between the core and cladding. While there are a number of possible reasons for this, including the evolution of the environment inside the core of the fiber (as reported in [26]), one possibility is the potential part pressurization (e.g. with 1.2-1.3 bar) of the cladding holes due to a non-ideal collapsing of the cladding holes combined with the time taken for the second splice, resulting in a subtle pressure equalization in the cladding during the first few hours. It is important to mention here that the equalization of pressure is within the cladding holes themselves, not between core and cladding as they are hermetically sealed.

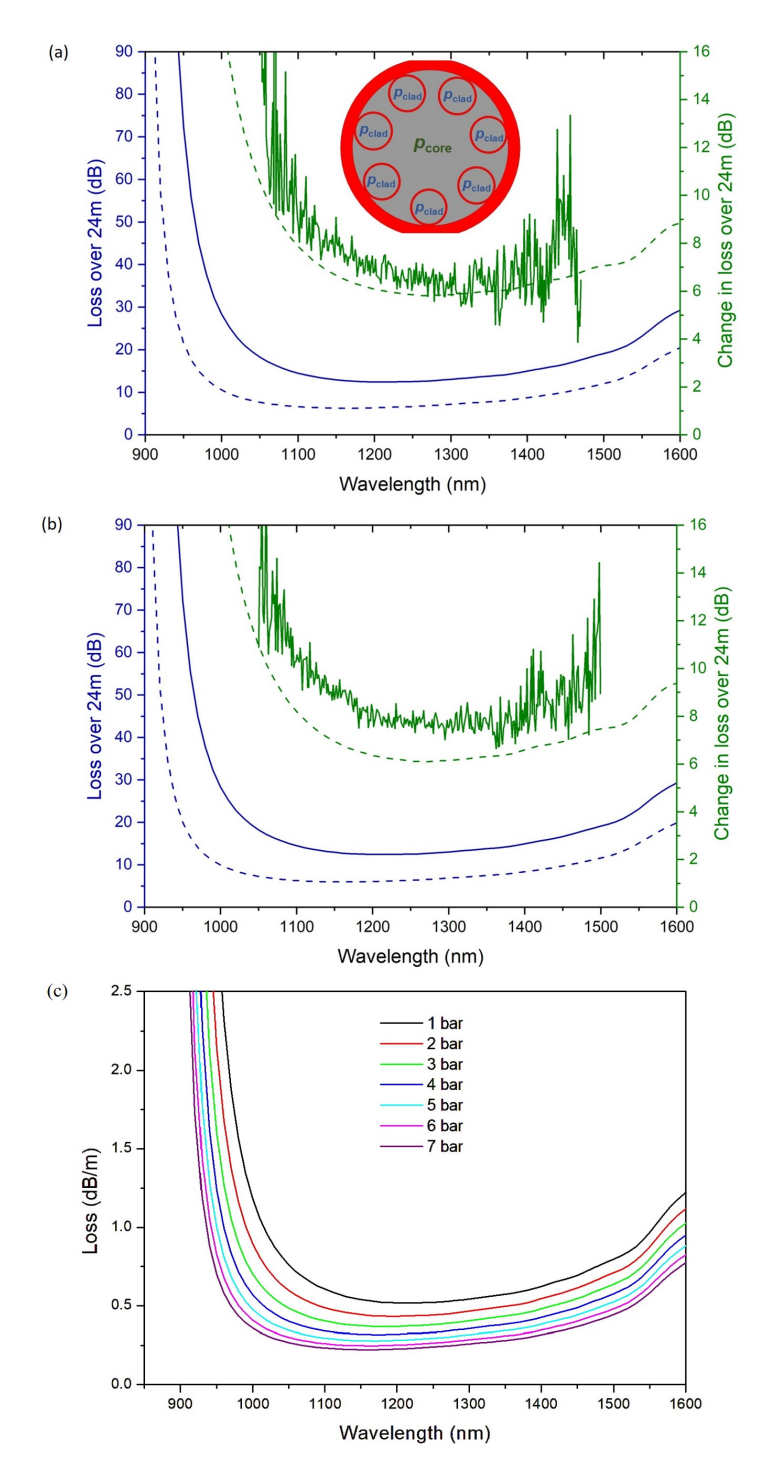


**Fig. 6.** Comparison between the modelled loss of the gas cells with differing core pressurization (blue lines, solid = 1 bar, dashed = 5.6/6 bar) and measured (solid green line) and modelled (dashed green line) change in loss with respect to the reference cell. Gas cell 1 is shown in (a) (inset: schematically shows pressure regions in core:  $P_{\rm core}$  and cladding:  $P_{\rm clad}$  of the HCF structure), core pressure,  $P_{\rm core}$ , = 5.6 bar. Gas cell 2 is shown in (b),  $P_{\rm core}$ , = 6 bar. In both cells cladding pressure,  $P_{\rm clad}$ , = 1 bar. For the reference cell,  $P_{\rm core} = P_{\rm clad} = 1$  bar. (c) Simulated confinement loss for selected values of core pressure while cladding pressure is fixed at 1 bar.

Figure 3(b) shows an apparent sudden change (improvement) in the transmission spectra of gas cell 2 between day 9 and 29. The stability of the cell's transmission before and after this change suggest it may have occurred as a single, potentially discrete change. Furthermore, there was no apparent change in any of the fibers (SMF, buffer, or hollow-core), their deployment, or the measurement set-up between the measurements on day 9 and 29. Due to a lack of information regarding the precise details of this change, it is hard to explain it with any certainty, especially as it could be attributed to a range of potential factors (either individually or collectively). However, from experience, sudden, discrete changes in coupling at splices can occur due to factors such as the relaxation of stresses inadvertently introduced at the splice point, or an unobserved subtle change in the bend condition of the buffer fiber (and hence its modality and/or beam profile) close to the splice point, and it is suspected this may be the cause here.

Given how consistent the transmission of both gas cells was outside of these effects (initial change in cell 1 and discrete change in cell 2) we do not believe either impacts the overall utility of this selective pressurization scheme, but further investigation is planned to attempt to understand both more fully. Table 1 summarizes all the gas cell measurements.

Table 1. Summary of improved optical properties of the gas cells due to selective gas filling

-	Gas pressure at core	Wavelength (nm)	Improvement (dB)	Time scale
Gas Cell 1	~ 5.6 bar	1100 nm	~ 8.5 dB (initial)	12 months (constant)
			$\sim 6.5 \text{ dB (after few hours)}$	
Gas Cell 2	~ 6.0 bar	1100 nm	$\sim 10 \text{ dB (initial)}$	12 months (constant)
			~ 11 dB (after 29 days)	

The reliability of this approach in terms of hermetic sealing can also be evaluated by consideration of the transmission spectra measured over 12 months. Periodic measurements over 12 months confirm that the transmission increase seen after 1 day (and/or 9-29 days for cell 2) are maintained for the full duration without any indication of gas permeation or leakage. The  $\sim 10$  dB enhancement at 1100 nm in the transmission of gas cell 2 indicates the reduction of loss by a factor of 3, from  $\sim 0.6$  dB/m to an estimated loss  $\sim 0.18$  dB/m, clearly demonstrating the significant effect GDRI can have on HCF optical performance. The HCF reported here is a simple tubular design, has higher confinement loss than more advanced designs (e.g., Nested Antiresonant Nodeless Hollow Core Fiber (NANF), Double Nested Antiresonant Nodeless Hollow Core Fiber (DNANF)) but GDRI can significantly improve the optical performance of the tubular fiber, and the selectively-core filled gas cells shown here demonstrate a practical route to do this.

## 5. Conclusion

In conclusion, hermetically sealed, selectively pressurized (positive core-cladding pressure difference) hollow-core fiber-based gas cells have been experimentally demonstrated for the first time. Measurements show that in the selectively-filled fabricated gas cells, the loss and bend sensitivity of the HCF is significantly reduced. A  $\sim$ 10 dB enhancement in the transmission at 1100 nm is achieved for  $\sim$ 6 bar core pressurisation, indicative of a reduction in loss by a factor of 3. The HCF's bend-loss performance is also dramatically enhanced allowing coiling to 4 cm bend diameter with minimal additional loss. Crucially, periodic measurements of the transmission of the gas cells indicate that these improvements in optical performance are maintained over at least 1 year with no indication of gas permeation between the core and the cladding regions and no leakage at the splice points. This work therefore demonstrates a practical, all-fiber format which can be used to exploit GDRI to improve the optical performance of a HCF. This opens up a practical means to significantly improve the optical performance of simple HCF designs like the tubular design tested here, potentially enabling competition with more complex state-of-the-art

nested fibers. Also, this approach could be particularly attractive for gas photonics applications requiring a compact footprint, such as high sensitivity gas detection, spectroscopy, non-linear optics, and frequency metrology.

**Funding.** Engineering and Physical Sciences Research Council (EP/N00762X/1, EP/P030181/1, EP/W037440/1); Royal Society (URF\R\211014).

**Disclosures.** The authors declare that there are no conflicts of interest related to this article.

**Data availability.** Data underlying the results presented in this paper are available from the University of Southampton repository at [29].

#### References

- 1. R. F. Cregan, B. J. Mangan, J. C. Knight, *et al.*, "Single-Mode Photonic Band Gap Guidance of Light in Air," Science **285**(5433), 1537–1539 (1999).
- 2. P. Russell, "Photonic Crystal Fibers," Science 299(5605), 358–362 (2003).
- 3. B. J. Mangan, M. Kuschnerov, J. W. Nicholson, *et al.*, "First demonstration of hollow-core fiber for intra data center low latency connectivity with a commercial 100Gb/s interface," in *Optical Fiber Communication Conference* (2015), paper M3D.4.
- 4. Y. Hong, K. R. H. Bottrill, T. D. Bradley, *et al.*, "Low-Latency WDM Intensity-Modulation and Direct-Detection Transmission Over >100 km Distances in a Hollow Core Fiber," Laser Photonics Rev **15**(9), 2100102 (2021).
- F. Poletti, N. V. Wheeler, M. N. Petrovich, et al., "Towards high-capacity fiber-optic communications at the speed of light in vacuum," Nat. Photonics 7(4), 279–284 (2013).
- M. Michieletto, J. K. Lyngsø, C. Jakobsen, et al., "Hollow core fibers for high power pulse delivery," Opt. Express 24(7), 7103–7119 (2016).
- S. Hanf, R. Keiner, D. Yan, et al., "Fiber-enhanced Raman multi-gas spectroscopy: a versatile tool for environmental gas sensing and breath analysis," Anal. Chem. 86(11), 5278–5285 (2014).
- M. Nikodem, G. Gomółka, M. Klimczak, et al., "Demonstration of mid-infrared gas sensing using an anti-resonant hollow core fiber and a quantum cascade laser," Opt. Express 27(25), 36350–36357 (2019).
- 9. P. Zhao, Y. Zhao, H. Bao, et al., "Mode-phase-difference photothermal spectroscopy for gas detection with an anti-resonant hollow-core optical fiber," Nat. Commun. 11(1), 847 (2020).
- P. S. J. Russell, P. Hölzer, W. Chang, et al., "Hollow-core photonic crystal fibers for gas-based nonlinear optics," Nat. Photonics 8(4), 278–286 (2014).
- F. Yang, F. Gyger, and L. Thévenaz, "Intense Brillouin amplification in gas using hollow-core waveguides," Nat. Photonics 14(11), 700–708 (2020).
- F. Benabid, F. Couny, J. C. Knight, et al., "Compact, stable and efficient all-fiber gas cells using hollow-core photonic crystal fibers," Nature 434(7032), 488–491 (2005).
- P. T. Marty, J. Morel, and Thomas Feurer, "All-Fiber Multi-Purpose Gas Cells and Their Applications in Spectroscopy,"
  J. Lightwave Technol. 28(8), 1236–1240 (2010).
- P. Jaworski, "Molecular dispersion spectroscopy in a CO2-filled all-fiber gas cells based on a hollow-core photonic crystal fiber," Opt. Eng. 58(02), 1 (2019).
- D. Suslov, T. W. Kelly, S. Rikimi, et al., "Towards Compact Hollow-Core Fiber Gas Cells," in Conference on Lasers and Electro Optics (2022), paper SW4 K.2.
- T. W. Kelly, P. Horak, I. A. Davidson, et al., "Gas-induced differential refractive index enhanced guidance in hollow-core optical fibers," Optica 8(6), 916–920 (2021).
- G. T. Jasion, J. S. Shrimpton, Y. Chen, et al., "Microstructure element method (MSEM): viscous flow model for the virtual draw of microstructured optical fibers," Opt. Express 23(1), 312–329 (2015).
- G. T. Jasion, J. R. Hayes, N. V. Wheeler, et al., "Fabrication of tubular anti-resonant hollow core fibers: modelling, draw dynamics and process optimization," Opt. Express 27(15), 20567–20582 (2019).
- 19. S. Pradhan, T. W. Kelly, I. A. Davidson, et al., "Enhancing the Optical Properties of Hollow Core Fiber Gas Cells by Selective Core Pressurisation," in *The European Conference on Lasers and Electro Optics* (2023), paper ce\_2\_5.
- R. Thapa, K. Knabe, K. L. Corwin, et al., "Arc fusion splicing of hollow-core photonic bandgap fibers for gas-filled fiber cells," Opt. Express 14, 9576–9583 (2006).
- C. Wang, R. Yu, B. Debord, et al., "Ultralow-loss fusion splicing between negative curvature hollow-core fibers and conventional SMFs with a reverse-tapering method," Opt. Express 29, 22470–22478 (2021).
- I. A. Davidson, M. Partridge, J. R. Hayes, et al., "Tubular anti-resonant hollow core fiber for visible Raman spectroscopy," in Proc. SPIE (2019), paper 112060R.
- Y Chen, M. N. Petrovich, E. N. Fokoua, et al., "Hollow Core DNANF Optical Fiber with <0.11 dB/km Loss," in Optical Fiber Communication Conference (2024), paper Th4A.8.
- R. Wynne and B. Barabadi, "Gas-filling dynamics of a hollow-core photonic bandgap fiber for nonvacuum conditions," Appl. Opt. 54(7), 1751–1757 (2015).
- Refractive Index common Liquids, Solids and Gases, https://www.engineeringtoolbox.com/refractive-indexd\_1264.html.

- 26. S. Rikimi, Y. Chen, T. D. Bradley, et al., "Long-term behaviour of water vapour absorption in hollow core fibers," in Sixth International Workshop on Specialty Optical Fibers and Their Applications (2019), paper 112061U.
- J. Henningsen and J. Hald, "Dynamics of gas flow in hollow core photonic band gap fibers," Appl. Opt. 47(15), 2790–2796 (2008).
- 28. T. W. Kelly, M. Mousavi, B. Shi, et al., "Coupling into higher order modes of a hollow-core fiber due to fusion splicing," in Conference on Lasers and Electro-Optics (2024), paper JW2A.73.
- 29. S. Pradhan, T. W. Kelly, E. Elistratova, *et al.*, "Dataset for Reduced Loss and Bend Sensitivity in Hermetically-sealed Hollow-core Fiber Gas Cells using Gas-induced Differential Refractive Index," University of Southampton (2024), https://doi.org/10.5258/SOTON/D3279.